Journal of Materials Chemistry C

PAPER

View Article Online
View Journal

Cite this: DOI: 10.1039/c8tc00554k

Bottom-up fabrication of graphene-based conductive polymer carpets for optoelectronics†

Tao Zhang,[a] Raul D. Rodriguez,*[bcd] Ihsan Amin,*[ace] Jacek Gasiorowski,[b] Mahfujur Rahaman,[b] Wenbo Sheng,[a] Jana Kalbacova,[bc] Evgeniya Sheremet,[bd] Dietrich R. T. Zahn[bc] and Rainer Jordan*[ac]

Received 1st February 2018,
Accepted 29th March 2018

DOI: 10.1039/c8tc00554k

rsc.li/materials-c

The covalent attachment of one dimensional (1D) polymer brush onto a two-dimensional (2D) material presents an appealing strategy to fabricate anisotropic polymer membranes, namely "polymer carpets". Conductive polymer carpets that are based on graphene and conductive polymers are especially interesting due to their potential in microelectronics, actuators and optoelectronics. Here we describe a versatile method for the covalent grafting of the poly(3-hexylthiophene) (P3HT) brush onto large area graphene to fabricate conductive polymer carpets through a combination of photografting polymerization and Kumada catalyst transfer polycondensation (KCTP) to grow P3HT (up to 260 nm) on single layer graphene forming conductive polymer carpets (*i.e.* G-PS-P3HT). Raman mapping revealed that the grafting reactions occurred on native graphene defects, without deteriorating the conjugation plane of graphene. The advanced architecture of G-PS-P3HT resulted in a high photocurrent (*ca.* 0.3 mA cm^{-2}) under light irradiation in a junction with MoS_2 to form efficient an p–n heterostructure, with promising potential in optoelectronics.

Introduction

The past decade has witnessed exciting progress in the development of two-dimensional (2D) organic/inorganic materials including graphene,[1] transition metal dichalcogenides[2] and 2D polymers.[3,4] These materials are recognized as promising candidates for the new generation of devices in many fields, including coatings, electronics and photo(electro)catalysis.[5–7] Recently, we introduced a new class of polymer material, namely "polymer carpets", as a large area and freestanding polymer brush on cross-linked self-assembled monolayers (SAMs),[8] graphene,[9] and polydopamine sheets.[10] Polymer carpets react spontaneously to environmental changes by *e.g.* swelling or shrinking of the brush, leading to dramatic changes of the optical, mechanical and surface properties (wetting, bioadhesion) of the entire carpet.[11,12]

To obtain graphene-based polymer carpets, polymer chains should be bound covalently to the graphene surface. However, the covalent attachment of functionalities can induce damage to the graphene lattice and degrade its electronic properties.[13] Recently, we demonstrated that vinyl monomers could be polymerized directly on single layer graphene *via* self-initiated photografting and photopolymerization (SIPGP).[9,14] The grafting was found to occur only at existing defect sites and does not impair the crystal quality and the consequent electronic properties of graphene. In this way, suitable monomers can be selected to design polymer brushes introducing additional functional groups that facilitate the further modification of graphene with various functionalities.[15]

Similar to graphene, conjugated polymers (CPs), and especially poly(3-alkylthiophenes) (P3AT), have drawn enormous interest due to their potentially low-cost, high-throughput fabrication methods.[16] The electronic and photonic properties of CPs are largely depending on their compact structure and morphology.[17] The use of CPs in solar cells,[18] light emitting diodes,[19] or sensors[20] often requires their covalent fixation on solid substrates.[21] Kumada catalyst transfer polycondensation (KCTP) has become a powerful tool in the synthesis of well-defined polythiophenes, polyfluorenes, their block copolymers,[22–25] as well as sophisticated donor–acceptor block copolymers[26–28] and star-branched polymers.[29–31] Recently, the KCTP was successfully adapted to surface-initiated polymerization, namely SI-KCTP, with external initiators to grow P3AT brushes on various substrates like

[a] *Chair of Macromolecular Chemistry, School of Science, Technische Universität Dresden, Mommsenstr. 4, 01062 Dresden, Germany. E-mail: raulmet@gmail.com, rainer.jordan@tu-dresden.de*
[b] *Semiconductor Physics, Technische Universität Chemnitz, 09107 Chemnitz, Germany*
[c] *Center for Advancing Electronics Dresden (cfaed), Technische Universität Dresden, Mommsenstr. 4, 01062 Dresden, Germany*
[d] *Tomsk Polytechnic University, 30 Lenin Ave, 634050 Tomsk, Russia*
[e] *Junior Research Group Biosensing Surfaces, Leibniz Institute for Plasma Science and Technology, INP Greifswald e.V., Felix-Hausdorff-Strasse 2, 17489 Greifswald, Germany. E-mail: ihsan.amin@inp-greifswald.de*

† Electronic supplementary information (ESI) available. See DOI: 10.1039/c8tc00554k

indium tin oxide (ITO),[32] gold,[33] glass,[34] Si wafers,[35] and graphene oxide.[18,36] In this process, the crucial step is to attach halogenated benzene (*e.g.* bromobenzene) on a target substrate, which could be furtherly converted to the Ni(II) macroinitiator for KCTP. Here, we show that P3HT brush layer can be grown on large-area single-layer graphene to form conductive polymer carpets through the combination of SIPGP and SI-KCTP. Raman spectroscopy shows that the grafting reaction occurred at the existing defects of graphene and without the introduction of additional defects. Photoluminescence mapping reveals a strong interaction between P3HT and graphene in the G-PS-P3HT carpets as compared to the cast P3HT films. The potential of the carpets in solar energy conversion is demonstrated by depositing a layer of n-type MoS_2 flakes onto G-PS-P3HT to build up p–n junction heterostructures.

Results and discussion

Synthesis of G-PS-P3HT carpet

Since graphene bears native sp^3 hybridized defects, the hydrogen from these defects sites can be abstracted upon UV irradiation, generating local radicals that initiate the free radical polymerization of 4-bromostyrene.[9,14] Thus, a thin layer of poly(4-bromostyrene) (PSBr) was obtained by SIPGP of 4-bromostyrene on single layer graphene grown *via* chemical vapor deposition (CVD) on Cu foil, as outlined in Fig. 1a. Under argon atmosphere, the substrate was immersed in a freshly distilled bulk 4-bromostyrene and irradiated for 40 min with UV light of a spectral range between 300 and 400 nm (intensity maximum at λ = 350 nm with a total power of *ca.* 5 mW cm^{-2}). After the polymerization, the substrate was rigorously rinsed with organic solvents to remove any physisorbed polymer. The covalently attached aryl bromide of PSBr on graphene undergoes an oxidative addition by placing it in a solution of $Ni(PPh_3)_4$.[34] The reaction is followed by the ligand exchange with the 1,3-bis(diphenylphosphino)propane (dppp), resulting in a surface-bound, metal-mediated coupling catalyst (Methods).[35] It is well known that dppp leads to the highest degree of the polymerization control in the P3HT synthesis in solution.[37] SI-KCTP was initiated by the addition of 2-bromo-5-chloromagnesio-3-hexylthiophene dissolved in tetrahydrofuran (THF). Afterwards, a thin layer of P3HT brush layer covering the entire graphene interface was observed. However, it is worth mentioning that the P3HT polymer is also formed in the bulk part of the solution. The polymer grown simultaneously in the solution was later precipitated with methanol, and used as a control material in the preparation of solution samples and cast films.[38,39] The polymer was analyzed by gel permeation chromatography (GPC) and ^{1}H NMR revealing a high percentage of regioregular head-to-tail (HT) linkage (>95%, Fig. S1, ESI†) and low dispersity ($Đ$ = 1.5 M_n = 12 kg mol^{-1}) (Fig. S2, ESI†).

The optical micrograph of a single layer graphene film transferred on a SiO_2/Si substrate is shown in Fig. 1b. The uniform

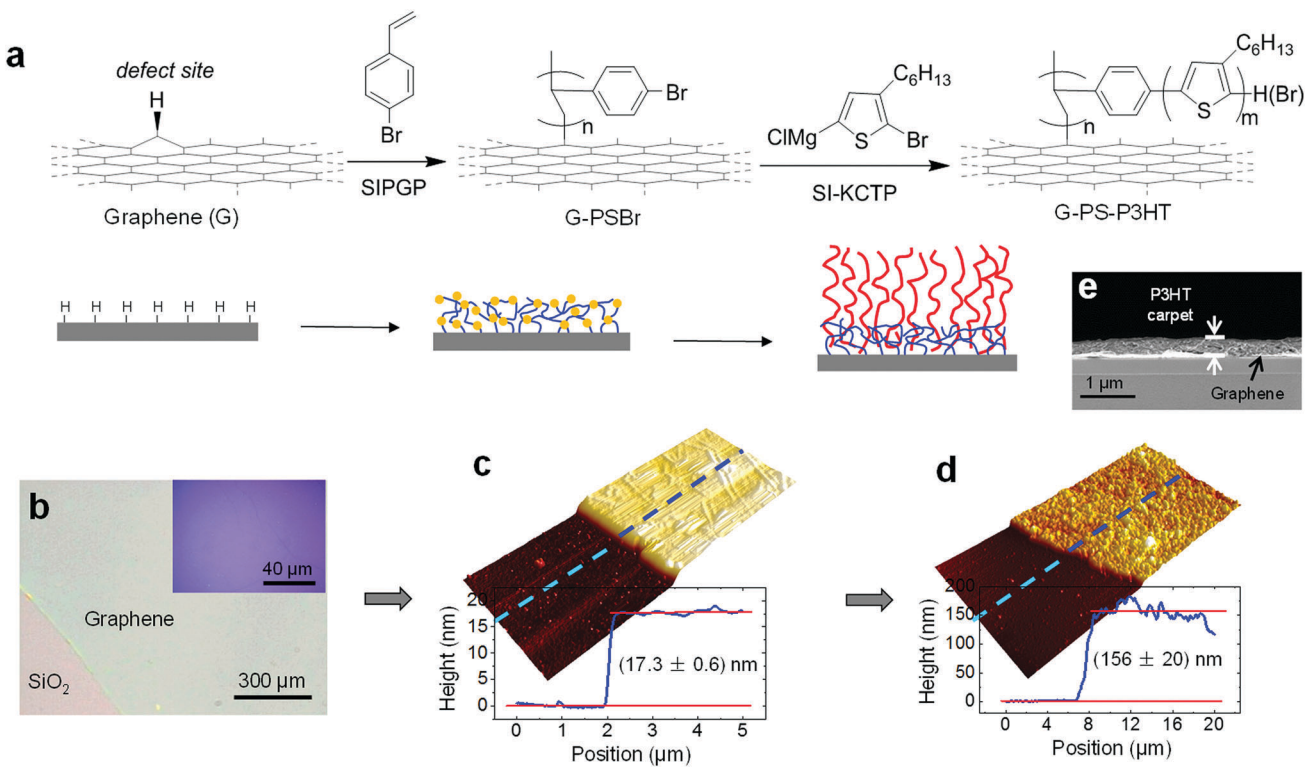

Fig. 1 Synthesis and morphology. (a) Schematic of the fabrication process of P3HT brushes on graphene. (b) Optical microscopy images of a CVD graphene transferred to the SiO_2/Si substrate, inset: close-up image. AFM images and height profiles along the dashed lines in the images for the (c) PSBr layer grown on graphene by SIPGP for 40 min, and (d) for the P3HT layer grown by SI-KCTP for 7 hours. (e) Scanning electron microscopy (SEM) cross-sectional image of the G-PS-P3HT carpet.

color contrast indicates the good macroscopic uniformity of the graphene. Atomic force microscopy (AFM) was used to monitor nanoscopic changes in feature dimensions due to the brush growth. Rippled structures caused by the difference between the thermal expansion coefficients of graphene and the Cu substrate during the CVD growth[40,41] was observed on the pristine graphene (Fig. S3, ESI†). The SIPGP makes a thin PSBr polymer layer (*ca.* 17 nm) on graphene, along with the characteristic wrinkles that are still visible in Fig. 1c. After the SI-KCTP, the AFM results clearly show that the P3HT layer increased the overall thickness to 156 nm (Fig. 1d). In addition, the film shows an expected root mean square (RMS) roughness of *ca.* 20 nm. The roughness might indicate that the grafting density is low (*ca.* 0.08 chains nm^{-2})[42] and so there are mushroom features on the surface,[43] or the polymer chains adopt a crystal-domain configuration,[44] similar to those of the other conjugated polymer brushes obtained by KCTP[32] or other Ni^0 mediated condensation polymerizations.[45] It is worthy of note that the layer thickness of both PSBr and P3HT can be controlled from a few nanometer up to *ca.* 200 nm by the reaction time (Fig. S4, ESI†). The scanning electron microscopy (SEM) cross-sectional image is presented in Fig. 1e. We can clearly distinguish the lower graphene sheet from the upper P3HT layer demonstrating the carpet-like morphology. Reference samples of pristine graphene on the Cu foil with no PSBr functionalization were exposed to identical reaction conditions. We did not observe any polymer growth on the surface after rinsing. This confirms the selectivity of the polymerization process and covalent character of the P3HT attachment for G-PS-P3HT. The presence of bromine and an increase of the carbon signal intensity in the X-ray photoelectron spectroscopy spectra of functionalized graphene, confirms the grafting of PSBr by SIPGP (Fig. S5, ESI†). Evidence of growing a P3HT brush layer can be obtained by the disappearance of bromine peaks and the emergence of sulfur peaks after SI-KCTP. Grazing incident X-ray diffraction (GI-XRD) of the G-PS-P3HT carpet shows a diffraction peak at $2\theta = 5.5 \pm 0.1^\circ$ for the (100) preferential orientation (Fig. S6, ESI†), ascribed to the edge-on orientation of the P3HT, which corresponds to the in-plane π–π stacking of the conjugated polymer rings and the out of plane stacking of the alkyl groups perpendicular to the substrate.[46,47] The current sensing atomic force microscopy (CS-AFM) experiments show that the G-PS-P3HT carpets exhibit semiconductor-like characteristics with a typical resistance of *ca.* 24 MΩ (Fig. S7, ESI†). The conductivity of the G-PS-P3HT was calculated to be of 0.03 S cm^{-1}, which is three orders of magnitudes higher than those of other un-doped P3HT films of 10^{-5} S cm^{-1}.[35,37,47]

μ-Raman spectroscopy characterization

Ideally, the graphene samples would be a uniform carbon lattice extending in two dimensions. In reality, the graphene sheets are heterogeneous due to the presence of wrinkles and grain boundaries. Such heterogeneities often remain unnoticed as predominantly Raman spectra from flat regions are measured. However, such defects are unavoidable in CVD grown graphene and contribute to the overall properties of the material. Therefore, we identified wrinkles and flat regions at two different areas of interest with distinct spectral features as shown in Fig. 2a. Wrinkles are in particular characterized by the presence of the D′ band around 1620 cm^{-1} indicating higher defect concentrations. Additional spectroscopic evidence of the high defect concentration in wrinkles is observed by the peak width (FWHM) increase of

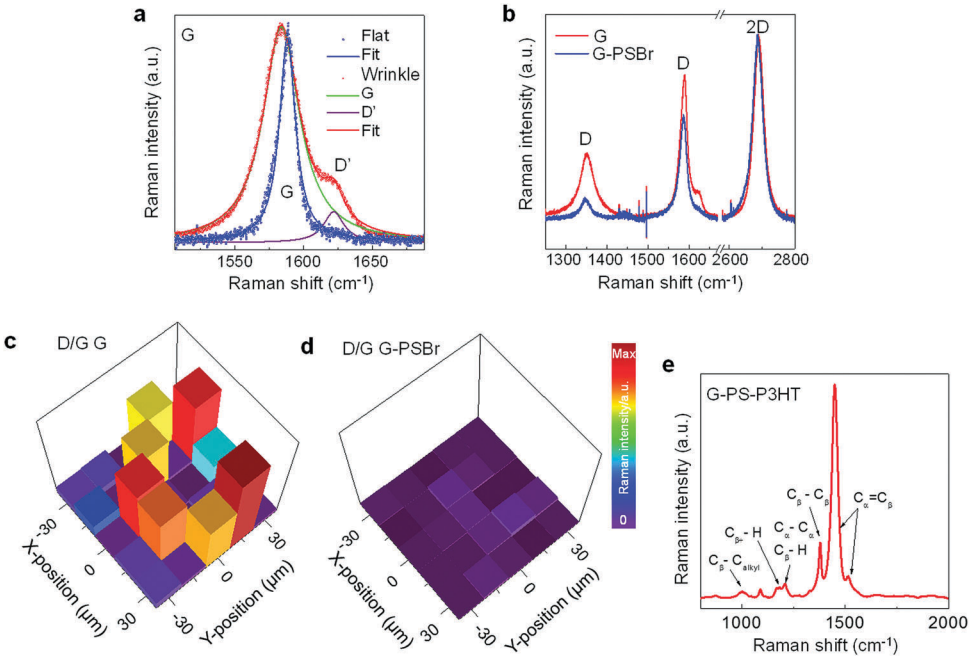

Fig. 2 Raman spectroscopy. (a) Heterogeneity in the normalized Raman spectra of pristine graphene comes from two distinct regions: flat and wrinkled. (b) Normalized average Raman spectra of pristine graphene and G-PSBr from 2278 individual spectra of both flat and wrinkled regions respectively. (c) Defect concentration represented by the D/G intensity ratio in a (60 × 60) μm^2 area before PSBr functionalization and (d) afterwards, revealing the defects dehydrogenation by PSBr on graphene as a decrease in the D/G intensity ratio.[48] (e) Chemical signature of P3HT in G-PS-P3HT.

the G band in Fig. 2a and by a high D band intensity. These observations result from the statistically averaged spectra from Raman maps covering all typical morphological structures (wrinkle, flat, and edge) on the graphene surface. A dedicated analysis of the role of wrinkles and edges on the chemical reactivity of graphene is being reported elsewhere.

Once the PSBr initiator reacts with graphene, we observe interesting changes in its vibrational properties deduced from the D/G intensity ratio in a 60 × 60 μm^2 graphene area (including wrinkles) before PSBr functionalization. As expected, the grafting of PSBr *via* SIPGP did not introduce additional defects on graphene (Fig. 2b).[9,14,49] However, the Raman intensity ratio (D/G) mapping (Fig. 2c and d) results suggest that the defect concentration of the whole graphene sheet (60 × 60 μm^2) decreased significantly in comparison to pristine graphene. These observations imply that the SIPGP of PSBr occurred on the graphene pristine defects.[9,14,48] This result can be understood as the following: the SIPGP process relies on hydrogen abstraction by photoactivated monomers and the grafting efficiency depends on the bond dissociation energy of the substrate surface (functional groups), and the hydrogen-terminal defects of sp^3 carbon on graphene are abstractable under the SIPGP conditions.[14,50] Therefore, no additional defects are required or induced during the reaction. The decrease in the D/G intensity ratio is in agreement with a previous report on the dehydrogenation of single-layer graphene[48] supporting our conclusion that these defects were used during the SIPGP reaction.[9,14] However, since PS substituted the hydrogenated sites in graphene, the defect concentration should remain the same. This apparent inconsistency can be explained by noticing that the relatively polar PSBr on graphene can induce localized charges. Even though disorder makes visible the D band in Raman, there are particular defects that do not activate the D band such as impurities that are electrically charged.[51,52] The change to the charged defects after PSBr results in the apparent decrease of defect concentration as seen from the D/G ratio. We verified that the graphene crystallinity remained unchanged by monitoring a simple parameter that is also another indication of disorder: the 2D peak width (Fig. S8, ESI†). We systematically observed that the 2D peak width of 38 cm^{-1} did not change after PSBr which further supports our hypothesis. Moreover, we observe a shift in the 2D band position in agreement with previous reports on electrostatic doping by charged impurities.[51,52] After the SI-KCTP, the Raman signatures of P3HT around 1450 cm^{-1} and 1380 cm^{-1} corresponding to the C=C and C–C vibrations of the thiophene ring are readily observed in the G-PS-P3HT carpet (Fig. 2e) confirming a successful polymer growth.[53,54]

Light absorption and emission

The P3HT brushes on graphene of G-PS-P3HT reproducibly displayed uniformly a brownish/red color across the substrate (Fig. 3a). The reference G-PSBr film on the copper foil shown on the left is the colorless reference sample. The G-PS-P3HT showed solvation chromism similar to free P3HT in solution. Their color changed from fuchsia in a good solvent (THF) to dark violet in a bad solvent (methanol), and finally to dull brownish in the dry state, due to a transition from the less (twisted) to a more (planar) conjugated conformation for regioregular P3HT.[34]

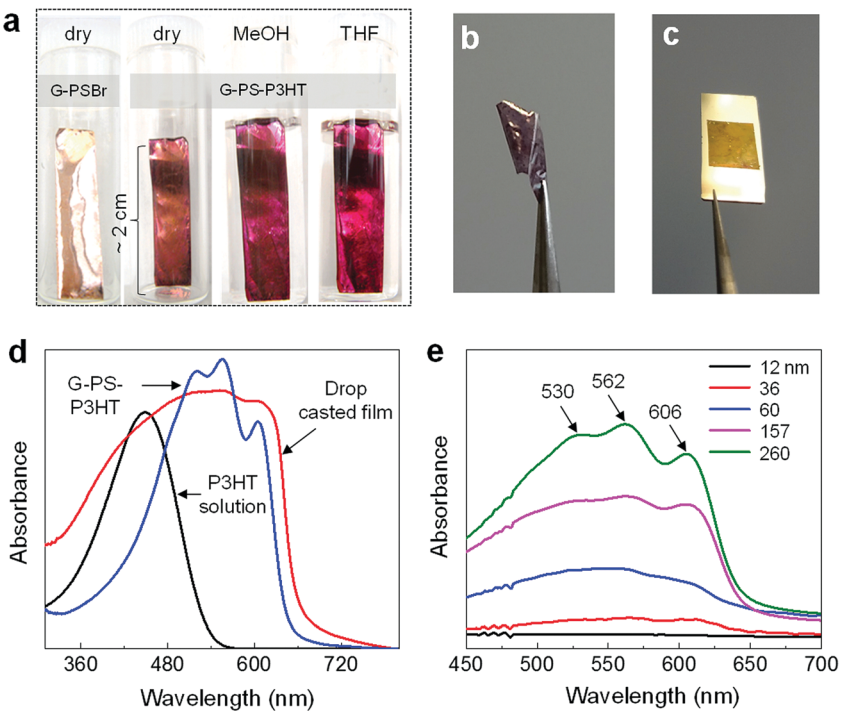

Fig. 3 Light absorption. (a) Photographs of graphene-PSBr on copper and after grafting with P3HT layer in the dry state and in two solvents (MeOH and THF). (b) The free-standing G-PS-P3HT carpet. (c) G-PS-P3HT on the Au/Si wafer. (d) UV/Vis spectra of P3HT dissolved in THF, drop-cast and grafted G-PS-P3HT. (e) UV-vis spectra of the G-PS-P3HT with different thicknesses. The thickness for the PSBr layer (*ca.* 17 nm) is identical for all the samples.

These results also imply the conformational freedom of P3HT chains despite the fact that they are tethered to the substrate. The G-PS-P3HT is mechanically robust and a free-standing polymer carpet was obtained by etching away the Cu foil (Fig. 3b), and the carpet can be simply transferred on any other substrates for various characterizations and applications, *e.g.* the Au/Si wafer as shown in Fig. 3c.

It is accepted that the increase of the degree of polymerization of regioregular P3HT results in a gradual bathochromic shift in the UV absorption spectra, especially in a bad solvent.[55,56] We observed that the G-PS-P3HT carpet of different thickness obtained by SI-KCTP have absorption intensities that systematically increases with the thickness as expected (Fig. 3e). In the sample with the thickest brush (260 nm), we observed the appearance of fine structure peaks in the regions around 528 nm and 605 nm. This is indicative of a progression of the π–π* transition related to the C=C vibrational transition, and is a characteristic of regioregular P3HT. It has been confirmed that these additional absorption peaks are related to the planarization of the conjugated system.[57,58] The polymer obtained from the same reaction solution was measured as a reference. As might be expected, the peaks due to inter-polymer interactions could not be observed when the P3HT was dissolved in THF, and are barely visible for P3HT cast films on the same substrate type (Fig. 3d).

By exciting the thin film with a laser (λ = 514.7 nm) in resonance with the absorption band, a photoluminescence (PL) emission covering a wide spectral range from the visible to the near infra-red was detected, which gave evidence for the P3HT/graphene interaction regarding the preparation methodologies. Reference P3HT samples were prepared by drop-casting on Au and on Au/G substrates. The cast films with similar thickness (*ca.* 200 nm) exhibited a low PL intensity band centered at 630 nm as can be seen from the first two curves in Fig. 4a. There is an obvious effect of the graphene interlayer in the PL emission for the drop-cast samples, since the graphene can enhance the crystallization of P3HT on its surface which has been demonstrated recently.[59,60] The covalently grafted G-PS-P3HT film shows a significant increase of the PL band intensity and broadening. In contrast, previous studies of the PL of P3HT-based graphene composites prepared by *ex situ* polymerization have shown a quenching effect.[61] The opposite effects on PL intensity are probably due to the covalent bonding nature of P3HT with graphene in the G-PS-P3HT carpet. Similar to our results, it has been reported that, in covalent bonded P3HT–graphene composites (prepared by *in situ* oxidative polymerization), the PL intensity increases with an increase in graphene concentration, and no photoluminescence quenching occurred.[62] The higher PL in the P3HT-based composites by *in situ* polymerization can be attributed to a more planar conformation of thiophene rings[63] or/and enhanced excitation based energy transfer from the graphene to the P3HT.[64] The strong enhancement in the PL intensity of G-PS-P3HT was further confirmed by measuring the PL intensity mapping of the patterned G-PS-P3HT carpet by plotting the emission intensity at 570 nm (Fig. 4b). There is a drastic difference in the PL intensity on the UV irradiated pattern on the graphene surface as visible from the color contrast of the PL map, which corroborates the Raman mapping and the AFM image of the patterned G-PS-P3HT (Fig. S9, ESI†).

G-PS-P3HT/MoS_2 heterostructure for light harvesting

The chemical grafting of P3HT has proven to be an excellent method to improve the PL of the polymer material which is a key parameter for the improvement of optoelectronic performance. However, low photoluminescence was found to be one of the main limitations for material choice in optoelectronics.[65] Given the correlation between PL and electroluminescence, the tuning of the PL emission suggests the potential of using the hybrid G-PS-P3HT carpets in optoelectronics such as light harvesting. We demonstrate this potential by studying a heterostructure made of G-PS-P3HT and MoS_2 flakes. The aim was to find out whether charge carriers can be dissociated at the interface. The schematic structure of the prepared device is shown in Fig. 5a. The AFM image in Fig. 5b shows one MoS_2 flake on the P3HT layer on which the measurements were performed. The monochromatic excitation for the *I–V* characterization was the same as used in the Raman and PL spectroscopic measurements, namely λ = 514.7 nm. This excitation energy matches a maximum in the absorption of P3HT (Fig. 3). The significant quenching of the PL shown in Fig. 5c suggests

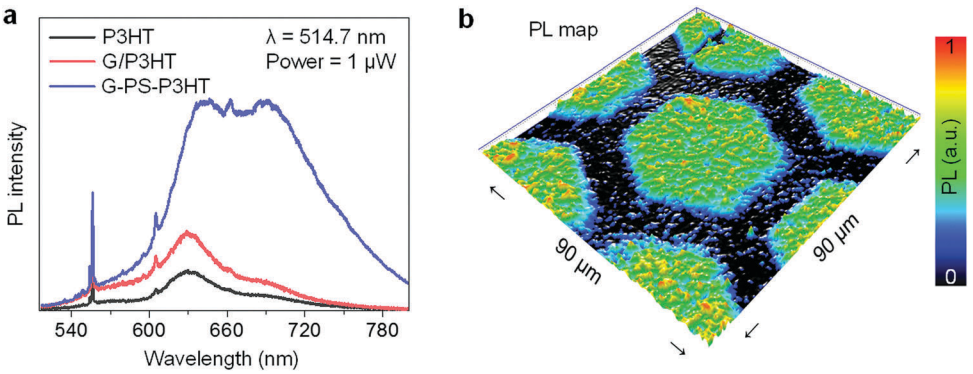

Fig. 4 Photoluminescence. (a) Photoluminescence (PL) spectra of G-PS-P3HT carpet and drop-cast P3HT on Au and Au/G under 514.7 nm excitation. The G-PS-P3HT carpet shows a much higher PL intensity and a broader PL spectral range as compared to drop-cast samples. All the films had similar thicknesses. (b) PL map of the patterned G-PS-P3HT carpet obtained by plotting the intensity at 570 nm under 514.7 nm excitation.

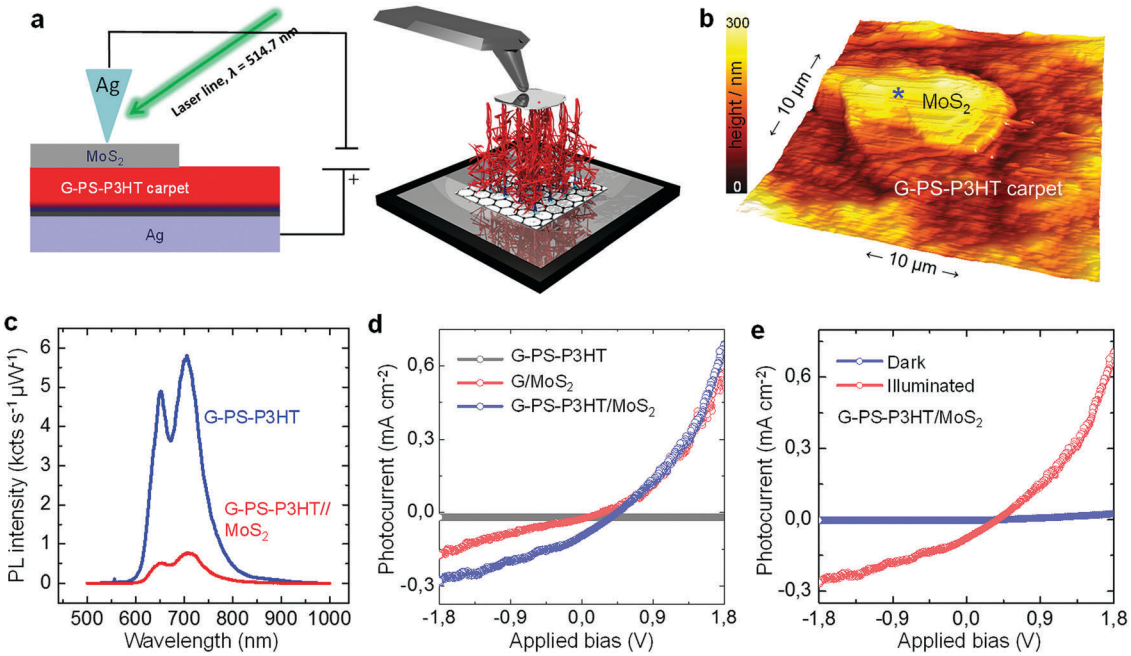

Fig. 5 Energy harvesting using a two-dimensional MoS_2 flake as an n-type material. (a) Schematics of the current sensing AFM (CSAFM) of the hybrid heterostructure under illumination. (b) AFM height scan of the region around a MoS_2 flake. The "*" marks the position where *I–V* curves in (d) were recorded. (c) The quenching of PL intensity from P3HT with MoS_2 evidences the charge-transfer between the two layers. (d) Photocurrent of G-PS-P3HT, MoS_2 on G-PS-P3HT and MoS_2 on graphene. The light conversion is evidenced by the photocurrent in the *I–V* curve shown in (e) with and without illumination at λ = 514.7 nm.

that efficient electron–hole separation occurs at the P3HT/MoS_2 p–n interface. The *I–V* characterization results demonstrate that the photocurrent can be strongly enhanced in the region where the MoS_2 is deposited (on G-PS-P3HT carpet) as compared to MoS_2 on graphene, while on the bare G-PS-P3HT carpet the current was negligible (Fig. 5b). Simultaneous topographic and current images were measured to confirm the significant enhancement in the photocurrent at the heterostructure (Fig. S10, ESI†). In addition, the variation of *I–V* curves under dark and illumination demonstrate the potential of the films for photoelectrocatalytic applications. The device exhibits pronounced photovoltaic behavior with a short-circuit photo current density of *ca.* 0.3 mA cm^{-2}, which is much larger than the results obtained from other MoS_2-based solar cells,[66,67] but lower than that of common solar cells,[68] which is likely attributed to the large roughness and poor contact of the interface. An interesting perspective is to quantify the efficiency of such solar cell, not only at the nanoscale but at the device level. Towards this demonstration, a better choice of the top electrode material and a suitable deposition approach should be achieved in order to ensure the appropriate energy band alignment for charge separation and diffusion. Also the characterization under full spectral illumination is to be investigated.

Conclusion

We demonstrate a robust and general methodology in the fabrication of conductive polymer carpets based on CVD graphene and P3HT using the combined surface-initiated polymerization means of SIPGP and SI-KCTP. Raman spectroscopy shows that the sp^2 and sp^3 nature of graphene is conserved after incorporation of the initiator and P3HT. The covalent grafting of P3HT on graphene produced stable conductive polymer carpets (*i.e.* G-PS-P3HT) that are mechanical robust and ready for transferring to arbitrary substrates. More importantly, the inter-chain absorption of P3HT was significantly improved as revealed by PL enhancement in contrast to the cast P3HT films. The energy harvesting capability was demonstrated by the generation of a photocurrent from the PL quenching of G-PS-P3HT with an n-type MoS_2 to form p–n heterostructures. We expect that the G-PS-P3HT carpet developed in this work is a promising material to manufacture a wide variety of flexible, highly conductive, and large-area electrodes potentially useful for optoelectronics.

Experimental

Materials

tert-Butyl magnesium chloride (1.0 M solution in THF), tetrakis(triphenylphosphine)nickel(0) ($Ni(PPh_3)_4$), 2,5-dibromo-3-hexylthiophene, 1,3-bis(diphenylphosphino)-propane, toluene (dry), THF (dry, stabilizer free) and chloroform were purchased from Sigma-Aldrich (Steinheim, Germany) and used as received. 4-Bromostyrene (97%, Sigma-Aldrich) was purified by passing through a basic alumina column to remove the inhibitor, degassed and distilled. Single-layer CVD graphene was purchased from the Graphene Supermarket (Graphene Laboratories Inc., Calverton, NY, USA) as 4″ × 2″ sheets on a 20 μm thick Cu foil and used as received. The quality of each sheet of being a single layer graphene was checked by Raman spectroscopy, AFM and optical microscopy.

Graphene transfer. For the transfer of pristine or functionalized graphene, the samples were spin-coated with PMMA (Allresist GmbH product no. AR-P671.04, dissolved in chlorobenzene) and cured at 90 °C for 10 min. The Cu substrate was etched away within 2 h by an aqueous solution of ammonium persulfate (0.25 g mL^{-1}). The PMMA/graphene film was rinsed with deionized water and transferred to the target substrate. PMMA was removed by thorough rinsing with acetone.

Poly(bromostyrene) (PSBr) brush on graphene

The PSBr grafting on graphene was performed analogously as described before with 4-bromostyrene.[9,14] After SIPGP, the samples were thoroughly rinsed with a series of solvents (toluene, ethyl acetate, and ethanol) to ensure that only chemically grafted PSBr remained on the substrate.

Poly(3-hexylthiophene) (P3HT) brush on PSBr

Grignard-functionalized monomer. Under dry argon, a dry flask was charged with 2,5-dibromo-3-hexylthiophene (214 μL, 0.96814 mmol) and anhydrous THF (10 mL). A 1 M solution of *tert*-butyl magnesium chloride in THF was added. The mixture was stirred at 32 °C for 24 h prior to use.

Surface-initiated Kumada catalyst transfer polycondensation (SI-KCTP). The catalyst solution was prepared in a glovebox, in an oven dried (120 °C, 4 h) flask with 20 mg of $Ni(PPh_3)_4$ dissolved with 20 mL of anhydrous toluene. The G-PSBr substrates were transferred into a tube with 1 mL of the catalyst solution (4.3×10^{-4} mmol mL^{-1}) and left up to 24 h. Afterwards, 1,3-bis(diphenylphosphino) propane (1 mg, 2.4×10^{-3} mmol) was added to the crude solution for ligand exchange. The solution was left for 2 h and 1 mL (9.6×10^{-2} mmol mL^{-1}) Grignard-functionalized monomer solution ($M_{monomer}/M_{Ni} = 220$) was added and the samples were shaken for 3 min. Polymerization occurred at r.t. for the times indicated. The samples were removed from the solution, washed with excess of THF for 5 min under shaking and finally rinsed extensively with THF, chloroform and ethanol (three cycles) to ensure that only covalently bound polymers remained on the samples. The P3HT formed in solution was collected by precipitation (methanol), filtration and again washing with methanol (3×15 mL), and drying in vacuum.

Micropatterned G-PS-P3HT carpet

Patterned PSBr polymer brushes were prepared as described above by SIPGP in bulk 4-bromostyrene using a 400 mesh Cu TEM grid as a photomask and consecutive SI-KCTP.

Deposition of thin MoS_2 flakes. Single crystals of MoS_2 were kindly provided by Dr Emmanuelle Lacaze, Institute des Nano-Sciences de Paris, France. The deposition and characterization of the thin flakes on the P3HT brush was performed as reported previously.[69]

Characterization

Atomic force microscopy (AFM) was performed with a custom-made NTEGRA AFM from NT-MDT (Moscow, Russia) in tapping mode using commercially available Si tips under ambient conditions. Current sensing AFM (CSAFM) was performed with an Agilent AFM 5420 (USA) in contact mode using custom-made silver cantilevers. UV spectra were recorded on a Perkin-Elmer Lambda 35 spectrometer. Raman and photoluminescence spectroscopy measurements were performed with a Horiba JY Labram HR800 spectrometer (France) under 514.7 nm laser excitation at a power of 1.5 μW using diffraction gratings of 600 lines per mm. Raman and PL mapping was performed with a Marzhäuser microscope scanning stage (Germany) using a 100× objective (N.A. 0.9). X-ray photoelectron spectroscopy was performed at a base pressure of 1.4×10^{-9} mbar with Mg K radiation at an operating power of 10 mA at 15 kV. Gel permeation chromatography (GPC) was performed using a UV-975 intelligent UV/vis detector (λ = 450 nm, JASCO) running under THF (25 °C, 1 mL min^{-1}) as eluent and calibrated against styrene standards (PSS, Mainz, Germany). ^1H NMR spectra were recorded on a Bruker DRX 500 spectrometer at r.t. with $CDCl_3$ as the solvent. Grazing incident X-ray diffraction was carried out for characterization of structural properties of the G-PS-P3HT carpet using a Bruker D8 Advance diffractometer. The measurement was carried out at an incident angle of omega = 0.5°, with data collection performed over a range of 4 to 40° 2-theta, at a step width of 0.02° and a time of 5 s per step.

Conflicts of interest

The authors declare no competing financial interest.

Acknowledgements

Financial support from the Cluster of Excellence ''Center for Advancing Electronics Dresden'' (cfaed) and the China Scholarship Council (CSC) from the People's Republic of China (PhD grant to T. Z.) is gratefully acknowledged. R. D. R. and E. S. acknowledge the DFG-Research Unit 1713 ''Sensoric Micro- and Nanosystems'' and the Tomsk Polytechnic University Competitiveness Enhancement Program grant. We acknowledge Dr Angela Kruth and Anja Albrecht (INP Greifswald) for XRD measurements. This work was performed in the context of the European COST Action MP1302 Nanospectroscopy.

References

1 K. S. Novoselov, A. K. Geim, S. V. Morozov, D. Jiang, Y. Zhang, S. V. Dubonos, I. V. Grigorieva and A. A. Firsov, *Science*, 2004, **306**, 666–669.
2 Q. H. Wang, K. Kalantar-Zadeh, A. Kis, J. N. Coleman and M. S. Strano, *Nat. Nanotechnol.*, 2012, **7**, 699–712.
3 H. Sahabudeen, H. Y. Qi, B. A. Glatz, D. Tranca, R. H. Dong, Y. Hou, T. Zhang, C. Kuttner, T. Lehnert, G. Seifert, U. Kaiser, A. Fery, Z. K. Zheng and X. L. Feng, *Nat. Commun.*, 2016, **7**, 13461.
4 M. J. Kory, M. Worle, T. Weber, P. Payamyar, S. W. van de Poll, J. Dshemuchadse, N. Trapp and A. D. Schluter, *Nat. Chem.*, 2014, **6**, 779–784.

5 L. Vicarelli, M. S. Vitiello, D. Coquillat, A. Lombardo, A. C. Ferrari, W. Knap, M. Polini, V. Pellegrini and A. Tredicucci, *Nat. Mater.*, 2012, **11**, 865–871.
6 D. Jariwala, V. K. Sangwan, L. J. Lauhon, T. J. Marks and M. C. Hersam, *ACS Nano*, 2014, **8**, 1102–1120.
7 M. Krishnamoorthy, S. Hakobyan, M. Ramstedt and J. E. Gautrot, *Chem. Rev.*, 2014, **114**, 10976–11026.
8 I. Amin, M. Steenackers, N. Zhang, A. Beyer, X. H. Zhang, T. Pirzer, T. Hugel, R. Jordan and A. Golzhauser, *Small*, 2010, **6**, 1623–1630.
9 M. Steenackers, A. M. Gigler, N. Zhang, F. Deubel, M. Seifert, L. H. Hess, C. H. Y. X. Lim, K. P. Loh, J. A. Garrido, R. Jordan, M. Stutzmann and I. D. Sharp, *J. Am. Chem. Soc.*, 2011, **133**, 10490–10498.
10 D. Hafner, L. Ziegler, M. Ichwan, T. Zhang, M. Schneider, M. Schiffmann, C. Thomas, K. Hinrichs, R. Jordan and I. Amin, *Adv. Mater.*, 2016, **28**, 1489–1494.
11 T. Chen, R. Ferris, J. M. Zhang, R. Ducker and S. Zauscher, *Prog. Polym. Sci.*, 2010, **35**, 94–112.
12 M. A. C. Stuart, W. T. S. Huck, J. Genzer, M. Muller, C. Ober, M. Stamm, G. B. Sukhorukov, I. Szleifer, V. V. Tsukruk, M. Urban, F. Winnik, S. Zauscher, I. Luzinov and S. Minko, *Nat. Mater.*, 2010, **9**, 101–113.
13 S. Niyogi, E. Bekyarova, M. E. Itkis, H. Zhang, K. Shepperd, J. Hicks, M. Sprinkle, C. Berger, C. N. Lau, W. A. Deheer, E. H. Conrad and R. C. Haddon, *Nano Lett.*, 2010, **10**, 4061–4066.
14 M. Seifert, A. H. R. Koch, F. Deubel, T. Simmet, L. H. Hess, M. Stutzmann, R. Jordan, J. A. Garrido and I. D. Sharp, *Chem. Mater.*, 2013, **25**, 466–470.
15 Q. H. Wang, Z. Jin, K. K. Kim, A. J. Hilmer, G. L. C. Paulus, C. J. Shih, M. H. Ham, J. D. Sanchez-Yamagishi, K. Watanabe, T. Taniguchi, J. Kong, P. Jarillo-Herrero and M. S. Strano, *Nat. Chem.*, 2012, **4**, 724–732.
16 S. Gunes, H. Neugebauer and N. S. Sariciftci, *Chem. Rev.*, 2007, **107**, 1324–1338.
17 N. Kiriy, E. Jahne, H. J. Adler, M. Schneider, A. Kiriy, G. Gorodyska, S. Minko, D. Jehnichen, P. Simon, A. A. Fokin and M. Stamm, *Nano Lett.*, 2003, **3**, 707–712.
18 D. S. Yu, Y. Yang, M. Durstock, J. B. Baek and L. M. Dai, *ACS Nano*, 2010, **4**, 5633–5640.
19 J. J. Zhang, Q. Zou and H. Tian, *Adv. Mater.*, 2013, **25**, 378–399.
20 D. T. McQuade, A. E. Pullen and T. M. Swager, *Chem. Rev.*, 2000, **100**, 2537–2574.
21 M. Aryal, K. Trivedi and W. C. Hu, *ACS Nano*, 2009, **3**, 3085–3090.
22 E. E. Sheina, J. S. Liu, M. C. Iovu, D. W. Laird and R. D. McCullough, *Macromolecules*, 2004, **37**, 3526–3528.
23 M. C. Iovu, E. E. Sheina, R. R. Gil and R. D. McCullough, *Macromolecules*, 2005, **38**, 8649–8656.
24 R. Miyakoshi, A. Yokoyama and T. Yokozawa, *J. Am. Chem. Soc.*, 2005, **127**, 17542–17547.
25 A. G. Sui, X. C. Shi, S. P. Wu, H. K. Tian, Y. H. Geng and F. S. Wang, *Macromolecules*, 2012, **45**, 5436–5443.
26 J. Wang and T. Higashihara, *Polym. Chem.*, 2013, **4**, 5518–5526.
27 J. Wang, C. Lu, T. Mizobe, M. Ueda, W. C. Chen and T. Higashihara, *Macromolecules*, 2013, **46**, 1783–1793.
28 J. Wang, M. Ueda and T. Higashihara, *ACS Macro Lett.*, 2013, **2**, 506–510.
29 M. J. Yuan, K. Okamoto, H. A. Bronstein and C. K. Luscombe, *ACS Macro Lett.*, 2012, **1**, 392–395.
30 T. Higashihara, S. Ito, S. Fukuta, S. Miyane, Y. Ochiai, T. Ishizone, M. Ueda and A. Hirao, *ACS Macro Lett.*, 2016, **5**, 631–635.
31 T. Higashihara, *Macromol. Chem. Phys.*, 2017, **218**, 1600434.
32 S. K. Sontag, G. R. Sheppard, N. M. Usselman, N. Marshall and J. Locklin, *Langmuir*, 2011, **27**, 12033–12041.
33 S. K. Sontag, N. Marshall and J. Locklin, *Chem. Commun.*, 2009, 3354–3356.
34 V. Senkovskyy, N. Khanduyeva, H. Komber, U. Oertel, M. Stamm, D. Kuckling and A. Kiriy, *J. Am. Chem. Soc.*, 2007, **129**, 6626–6632.
35 N. Khanduyeva, V. Senkovskyy, T. Beryozkina, V. Bocharova, F. Simon, M. Nitschke, M. Stamm, R. Grotzschel and A. Kiriy, *Macromolecules*, 2008, **41**, 7383–7389.
36 Y. Sang, M. Fang and H. B. Lu, *Acta Polym. Sin.*, 2012, 223–230.
37 H. A. Bronstein and C. K. Luscombe, *J. Am. Chem. Soc.*, 2009, **131**, 12894–12895.
38 M. Ejaz, K. Ohno, Y. Tsujii and T. Fukuda, *Macromolecules*, 2000, **33**, 2870–2874.
39 K. Ohno, T. Morinaga, K. Koh, Y. Tsujii and T. Fukuda, *Macromolecules*, 2005, **38**, 2137–2142.
40 X. S. Li, W. W. Cai, J. H. An, S. Kim, J. Nah, D. X. Yang, R. Piner, A. Velamakanni, I. Jung, E. Tutuc, S. K. Banerjee, L. Colombo and R. S. Ruoff, *Science*, 2009, **324**, 1312–1314.
41 K. S. Kim, Y. Zhao, H. Jang, S. Y. Lee, J. M. Kim, K. S. Kim, J. H. Ahn, P. Kim, J. Y. Choi and B. H. Hong, *Nature*, 2009, **457**, 706–710.
42 T. Zhang, Y. H. Du, F. Muller, I. Amin and R. Jordan, *Polym. Chem.*, 2015, **6**, 2726–2733.
43 H. Q. Huang, S. E. Rankin, L. S. Penn, R. P. Quirk and T. H. Cheong, *Langmuir*, 2004, **20**, 5770–5775.
44 R. J. Kline, M. D. Mcgehee and M. F. Toney, *Nat. Mater.*, 2006, **5**, 222–228.
45 S. B. Jhaveri, J. J. Peterson and K. R. Carter, *Langmuir*, 2009, **25**, 9552–9556.
46 B. Kadem, A. Hassan, M. Goksel, T. Basova, A. Senocak, E. Demirbas and M. Durmus, *RSC Adv.*, 2016, **6**, 93453–93462.
47 J. H. Park, J. S. Kim, J. H. Lee, W. H. Lee and K. Cho, *J. Phys. Chem. C*, 2009, **113**, 17579–17584.
48 D. C. Elias, R. R. Nair, T. M. G. Mohiuddin, S. V. Morozov, P. Blake, M. P. Halsall, A. C. Ferrari, D. W. Boukhvalov, M. I. Katsnelson, A. K. Geim and K. S. Novoselov, *Science*, 2009, **323**, 610–613.
49 L. H. Hess, A. Lyuleeva, B. M. Blaschke, M. Sachsenhauser, M. Seifert, J. A. Garrido and F. Deubel, *ACS Appl. Mater. Interfaces*, 2014, **6**, 9705–9710.
50 J. Hong, J. B. Lee, S. Lee, J. Seo, H. Lee, J. Y. Park, J. H. Ahn, T. I. Seo, T. Lee and H. B. R. Lee, *NPG Asia Mater.*, 2016, **8**, e262.
51 C. Casiraghi, S. Pisana, K. S. Novoselov, A. K. Geim and A. C. Ferrari, *Appl. Phys. Lett.*, 2007, **91**, 233108.

52 M. Bruna, A. K. Ott, M. Ijäs, D. Yoon, U. Sassi and A. C. Ferrari, *ACS Nano*, 2014, **8**, 7432–7441.
53 W. C. Tsoi, D. T. James, J. S. Kim, P. G. Nicholson, C. E. Murphy, D. D. C. Bradley, J. Nelson and J. S. Kim, *J. Am. Chem. Soc.*, 2011, **133**, 9834–9843.
54 S. Falke, P. Eravuchira, A. Materny and C. Lienau, *J. Raman Spectrosc.*, 2011, **42**, 1897–1900.
55 M. Trznadel, A. Pron and M. Zagorska, *Macromolecules*, 1998, **31**, 5051–5058.
56 N. Khanduyeva, V. Senkovskyy, T. Beryozkina, M. Horecha, M. Stamm, C. Uhrich, M. Riede, K. Leo and A. Kiriy, *J. Am. Chem. Soc.*, 2009, **131**, 153–161.
57 M. C. Gurau, D. M. Delongchamp, B. M. Vogel, E. K. Lin, D. A. Fischer, S. Sambasivan and L. J. Richter, *Langmuir*, 2007, **23**, 834–842.
58 L. G. Li, G. H. Lu and X. N. Yang, *J. Mater. Chem.*, 2008, **18**, 1984–1990.
59 V. Skrypnychuk, N. Boulanger, V. Yu, M. Hilke, S. C. B. Mannsfeld, M. F. Toney and D. R. Barbero, *Adv. Funct. Mater.*, 2015, **25**, 664–670.
60 V. Skrypnychuk, N. Boulanger, V. Yu, M. Hilke, M. F. Toney and D. R. Barbero, *J. Mater. Chem. C*, 2016, **4**, 4143–4149.
61 Q. Liu, Z. F. Liu, X. Y. Zhong, L. Y. Yang, N. Zhang, G. L. Pan, S. G. Yin, Y. Chen and J. Wei, *Adv. Funct. Mater.*, 2009, **19**, 894–904.
62 F. Abd Wahab, K. Sulaiman and N. M. Huang, *J. Electron. Mater.*, 2013, **42**, 2739–2742.
63 X. Bai and S. Holdcroft, *Macromolecules*, 1993, **26**, 4457–4460.
64 S. J. Henley, R. A. Hatton, G. Y. Chen, C. Gao, H. L. Zeng, H. W. Kroto and S. R. P. Silva, *Small*, 2007, **3**, 1927–1933.
65 G. Li, V. Shrotriya, J. S. Huang, Y. Yao, T. Moriarty, K. Emery and Y. Yang, *Nat. Mater.*, 2005, **4**, 864–868.
66 M. Shanmugam, T. Bansal, C. A. Durcan and B. Yu, *Appl. Phys. Lett.*, 2012, **100**, 011111.
67 M. Shanmugam, C. A. Durcan and B. Yu, *Nanoscale*, 2012, **4**, 7399–7405.
68 S. Holliday, R. S. Ashraf, A. Wadsworth, D. Baran, S. A. Yousaf, C. B. Nielsen, C. H. Tan, S. D. Dimitrov, Z. R. Shang, N. Gasparini, M. Alamoudi, F. Laquai, C. J. Brabec, A. Salleo, J. R. Durrant and I. McCulloch, *Nat. Commun.*, 2016, **7**, 11585.
69 R. D. Rodriguez, S. Muller, E. Sheremet, D. R. T. Zahn, A. Villabona, S. A. Lopez-Rivera, P. Tonndorf, S. M. de Vasconcellos and R. Bratschitsch, *J. Vac. Sci. Technol., B*, 2014, **32**, 04E106.